ISBN: 978-3-95450-247-9 ISSN: 2673-5490 doi: 10.18429/JACoW-IPAC2024-THPR63

THERMAL DIFFUSIVITY AND ACOUSTIC PROPERTIES OF Nb THIN FILMS STUDIED BY TIME-DOMAIN THERMOREFLECTANCE

Md. Obidul Islam†, Hani E. Elsayed-Ali, Department of Electrical and Computer Engineering, Old Dominion University, Norfolk, Virginia 23529, USA and Applied Research Center, 12050 Jefferson Avenue, Newport News, VA 23606, USA

Abstract

The diffusion and acoustic properties of 200–800 nm thick Nb films deposited on Cu were investigated using time-domain thermoreflectance (TDTR). The Nb film grain size and thermal diffusivity decreased with reduced film thickness. As the film thickness was reduced from 800 nm to 200 nm, the thermal diffusivity decreased from 0.237± 0.002 cm^2s^{-1} to 0.100± 0.002 cm^2s^{-1} while the average grain size decreased from 65±16 nm to 20±6 nm. Damped periodic photoacoustic signal was detected due to laser heating generated stress in the Nb film which resulted in an acoustic pulse bouncing in the Nb film at the Cu and vacuum interfaces. The period of the acoustic oscillation gives a longitudinal sound velocity of 4247±72 ms^{-1} for the Nb film, which is in good agreement with the values reported in the literature.

INTRODUCTION

Superconducting radiofrequency (SRF) cavities used in particle accelerators are mostly made from high-purity bulk Nb [1]. These cavities have reached their performance limit since bulk Nb SRF cavities operate with accelerating fields that are very close to the superheating field of Nb [2]. Researchers are working towards cost-effective production of SRF cavity material, such as medium grain Nb discs sliced from forged and annealed billets, which could be useful in applications requiring high quality factors (Q_0) with moderate field gradients (~20 MV/m) [3]. The cavity performance is limited by the thermal breakdown of the superconductivity, which depends on the thermal conductivity of the cavity material [4]. Nb-coated Cu cavities have emerged as an alternative to bulk Nb for SRF cavity applications because of the high thermal conductivity of Cu and the relative ease of forming the cavity structure [5, 6, 7]. Critical factors affecting the performance of a coated SRF cavity include Nb thin film thickness, surface defects, grain size, and the Nb/Cu thermal interface resistance.

TDTR uses ultrafast lasers to excite thin films and measure their thermal properties, such as thermal diffusivity and interfacial thermal conductance [8, 9, 10]. In TDTR, a probe laser pulse, delayed from the pump pulse, measures changes in sample reflectance at various delay times between the pump and the probe. These changes in the optical properties reflect the temporal evolution of electron temperature (T_e) and lattice temperature (T_l). The thermal diffusivity is determined by fitting the TDTR signal recorded after electron-phonon thermalization to a temperature decay model derived from Fourier heat conduction law [11]. Several investigations have studied the thermal characteristics and response to ultrafast heating of Nb thin films [9, 12, 13, 14]. Microstructural properties and surface morphology also influence the thermal properties and SRF cavity. For instance, intragranular impurities reduce the electron mean free path and the local critical field, while grain boundaries serve as scattering centers. Enhancing the grain size of Nb films on Cu and reducing surface defects was demonstrated to enhance the superconducting properties of Nb thin films [15]. Absorption of laser pulses generates elastic stress, resulting in periodic oscillations in the TDTR signal. This ultrasonically modulated TDTR signals can be used to determine the sound velocity in the film [16, 17]. We conducted TDTR measurements to measure the thermal diffusivity of 200–800 nm Nb films deposited on Cu at room temperature. We also measured the sound velocity in these films by picosecond photoacoustic.

EXPERIMENTAL SETUP

The Nb films were deposited on Cu using a DC magnetron sputtering system (AJA ATC Orion 5). The Nb sputter target had a purity of 99.99%, a diameter of 2 inches, and a thickness of 0.25 inches. Prior to deposition, the deposition chamber was evacuated to a base pressure of ~3×10^{-5} Pa. Deposition took place at a pressure of 0.4 Pa, using 99.999%-pure argon with a flow rate of 20 SCCM. The substrate was kept at room temperature and was rotated at 30 rpm during deposition. The deposition rate, set at 0.8 Å/s, was calibrated using a crystal thickness monitor positioned at the substrate location before deposition. The film surface morphology was examined using field-emission scanning electron microscopy (SEM) with a 15 kV accelerating voltage.

The TDTR setup uses a Ti:sapphire laser oscillator (wavelength λ = 800 nm, pulse duration τ ~110 fs, and a repetition rate 80 MHz). This laser beam is split by a non-polarizing beam splitter into a pump beam and a probe beam, maintaining an intensity ratio of 9:1. The energy of the pump pulse is ~1.25 nJ. The pump beam undergoes modulation at a frequency of 600 kHz via an acousto-optic modulator (AOM). Both the pump and probe beams are focused tightly onto the sample surface using a 10X lens, with the pump and probe beam diameters ~20 μm and ~10 μm ($1/e^2$), respectively, as determined by an optical beam profiler. The pump beam strikes the sample surface perpendicularly, while the probe beam is incident at a 3° angle from the surface normal. The reflected probe beam is captured by a Si photodiode detector, with a polarizer positioned before the detector to block the scattered S-polarized pump beam. The normalized change in probe-beam reflectance ($\Delta R/R$) is measured using a lock-in amplifier. More details on the TDTR setup were given previously [8].

Content from this work may be used under the terms of the CC BY 4.0 licence (© 2024). Any distribution of this work must maintain attribution to the author(s), title of the work, publisher, and DOI.

ISBN: 978-3-95450-247-9 ISSN: 2673-5490 doi: 10.18429/JACoW-IPAC2024-THPR63

© Content from this work may be used under the terms of the CC BY 4.0 licence (© 2024). Any distribution of this work must maintain attribution to the author(s), title of the work, publisher, and DOI.

RESULTS AND DISCUSSION

The femtosecond laser is absorbed within the skin depth of the laser wavelength in Nb leading to changes in the dielectric constant of Nb, affecting the sample's reflectance. Under the condition of weak excitation, $\Delta R/R$ is considered proportional to $T_e = T_l$ for small temperature excursions [18]. Because the laser spot size is significantly larger than the optical skin depth, thermal diffusion in directions parallel to the surface is regarded as negligible throughout the duration of the measurement [12]. The 1D heat diffusion model following Fourier's law is given by Eq. (1) [19].

$$\frac{\partial T(z,t)}{\partial t} = \alpha \frac{\partial^2 T(z,t)}{\partial z^2} + \frac{S(z,t)}{C\rho}, \quad (1)$$

where, $T(z, t)$ is the temperature profile, z is the distance normal to the film surface, C is the specific heat capacity in $Jkg^{-1}K^{-1}$, α is the thermal diffusivity in cm^2s^{-1}, ρ is the mass density of the sample in kgm^{-3}, and $S(z,t)$ is the laser source term ($Jm^{-3}s^{-1}$). The laser source function exhibits a Gaussian profile in time and decays exponentially as given by Eq. (2) [11, 20, 21]:

$$S(z,t) = (1-R)\frac{J}{t_p d}\exp\left[-\frac{z}{d} - 2.77\left(\frac{t}{t_p}\right)^2\right], \quad (2)$$

where R is the reflectance of the Nb film, J is the laser fluence in Jm^{-2}, d is the skin depth of Nb at 800 nm, and t_p is the laser pulse width. The product of specific heat capacity C and mass density ρ is the volumetric heat capacity. For Nb, the volumetric heat capacity is $C_l = C\rho = 2.3 \times 10^6$ $Jm^{-3}K^{-1}$ and $d = 20$ nm for 800 nm wavelength [9, 12]. The pump laser fluence was ~ 3.98 Jm^{-2} and the reflectance measured for the films was $R \sim 0.9$ for all film thicknesses studied. In 1D heat diffusion model, the initial sample temperature is set to 293 K and the heat flux at boundaries was assumed to be zero. The basis of this assumption is the negligible heat loss at the Nb/vacuum interface and the minimal heating of the Nb/Cu interface by the ultrafast laser pulse due to the rapid decay of the heat pulse over the Nb film thickness perpendicular to the surface.

Table 1: Thermal diffusivity and grain size of Nb films.

Thickness (nm)	Thermal diffusivity (cm^2s^{-1})	Grain size (nm)
800	0.237± 0.002	65±16
400	0.225 ± 0.002	43±10
200	0.100 ± 0.002	20±6

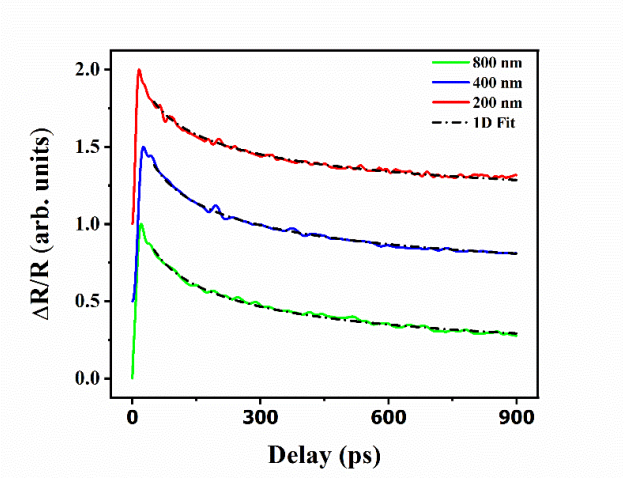

Figure 1: TDTR scans from Nb films of different thicknesses fitted with 1D heat diffusion model from time delay 50–900 ps between the pump and probe laser pulses.

Figure 1 shows $\Delta R/R$ from the 200, 400, 800 nm Nb films on Cu substrates. All data were averaged over 5 scans, and a 5-point FFT filtering was applied. The thermal diffusivity of the Nb films was determined by fitting the $\Delta R/R$ scans for time delays from 50 to 900 ps between the pump and probe laser pulses. The value of α for the 800 nm films (α = 0.237± 0.002 cm^2s^{-1}) is similar to that reported for bulk Nb [12]. For the 400 and 200 nm films, α has values of 0.225 ± 0.002 and 0.100 ± 0.002, respectively. The thermal diffusivity of other thin film materials was previously reported to be significantly reduced compared to their bulk counterparts [22, 23]. This reduction in thermal diffusivity with decreased thickness was linked to the reduced grain size of the thin films. SEM micrographs of the surface of the Nb films are shown in Fig. 2. The average grain size for each film is determined from a dataset comprising 50 grains. The measured grain size and α of Nb films of different thicknesses are displayed on Table 1. The observed trend of increased grain size with increasing film thickness is consistent with previously reported results for Nb films [24, 25].

Absorption of the laser pulse causes thermal expansion and resulting in an acoustic waves of ultrasonic frequency propagating away from the free surface at the longitudinal sound speed. The pulse is reflected at the boundary with the substrate and returns to the front surface after a time $t = 2d/v$, where d is the thickness of the film and v is the

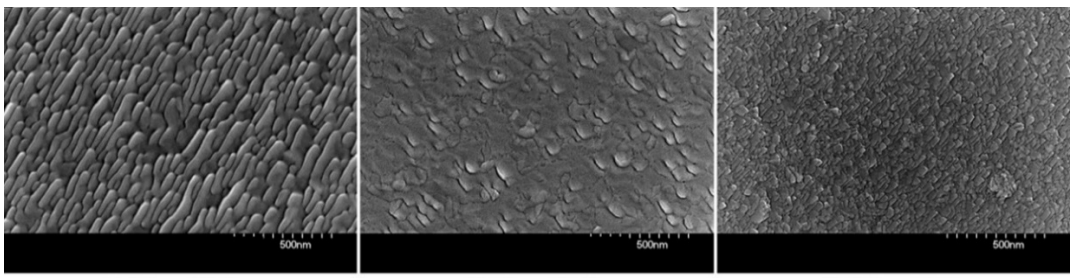

Figure 2: SEM images of the surface of Nb films of different thicknesses: (a) 800 nm, (b) 400 nm, (c) 200 nm Nb films.

ISBN: 978-3-95450-247-9 ISSN: 2673-5490 doi: 10.18429/JACoW-IPAC2024-THPR63

longitudinal sound velocity. The TDTR scans showing the acoustic oscillations measured from 800, 400 and 200 nm Nb films are displayed in Fig. 3. The period of the oscillations varies linearly with the film thickness. Acoustic echoes were also observed in metals like Cu, Al and Ni [26].

Table 2: Sound velocity measured for Nb films.

d, estimated. (nm)	d, measured. (nm)	t (ps)	v (ms^{-1})
800	660	305	4328
400	385	182	4231
200	230	110	4182

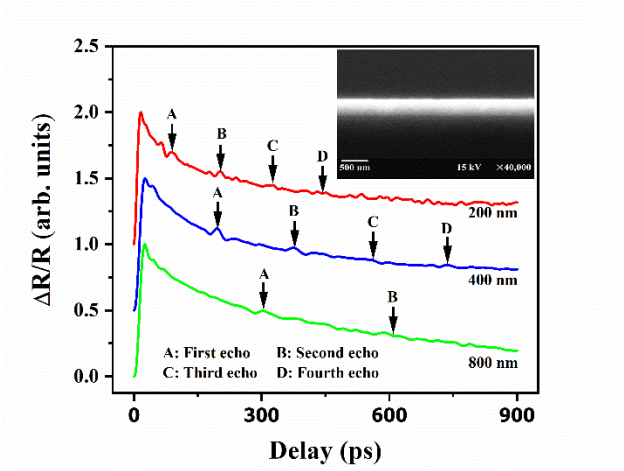

Figure 3: TDTR scans from Nb films of different thicknesses show the acoustic oscillations in the thermoreflectance signal. The inset shows the cross-sectional SEM image of 400 nm Nb film on Cu substrate.

To determine v for Nb films, the thickness of the films is measured, and the period of the acoustic oscillations is obtained from the TDTR signals. The accuracy of the film thickness estimated from the deposition rate using a crystal thickness monitor is checked by depositing the films on Si wafer under the same deposition conditions followed by cleaving the Si wafer and then obtaining the cross-sectional SEM. The inset in Fig. 3 shows the cross-sectional SEM image of the 400 nm film, giving the more accurate thickness of 385 nm. For the 400 nm film the period of the acoustic oscillations is measured to be 182 ps and the value of v is calculated to be 4231 ms^{-1}. The thickness measured for each film and the values of v calculated are summarized on Table 2. The average value of v for the three Nb films is 4247±72 ms^{-1}. Our calculated value of v in Nb agrees with the value (3480–4900 ms^{-1}) reported by Shabalin [27].

The heat diffusion time for the Nb films of thicknesses 200–800 nm ranges from ~1.7–27.0 ns, which are longer than our maximum observation time of 900 ps. Therefore, the effect of the Nb/Cu interface on heat transport is insignificant in our measurement. However, the acoustic wave of ultrasonic frequency can pass through the Nb films multiple times for the thickness range studied. To investigate the impact of interfaces on acoustic properties, Nb films with a thickness of 400 nm were grown on two different Cu substrates: polished 3 mm bulk Cu and a 1 μm thick Cu film deposited on sapphire. Figure 4 shows the TDTR signals from these two Nb films on different Cu substrates, with an inset showing atomic force microscopy (AFM) images of the two Cu substrates. Although both films exhibit the same thermal diffusivity, no acoustic echoes were detected in the TDTR signal obtained from the Nb film deposited on the 1 μm thick Cu substrate. The root mean square (rms) surface roughness measurements for the Cu substrates were 0.665 nm for the bulk Cu and 5.49 nm for the 1 μm Cu substrate. Substrate roughness plays a significant role in adhesion in thin film interfaces, impacting factors such as film uniformity, stress distribution, and interfacial bonding. Surface roughness affects the coherence of the reflected acoustic pulse with a rough surface diminishing its appearance.

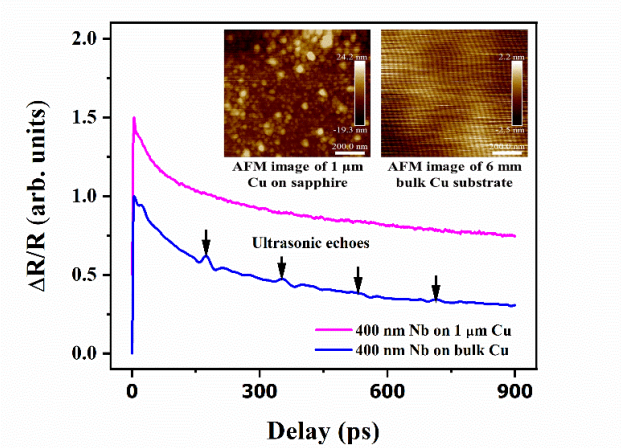

Figure 4: TDTR scans from 400 nm Nb films deposited on two different Cu substrates: 3 mm thick bulk Cu and 1 μm Cu thin film deposited on sapphire. The AFM images in the inset display the surface of the two Cu substrates used.

CONCLUSION

The thermal diffusivity α of Nb films was measured by TDTR fitted to a 1D heat diffusion model. Reduction of α is observed when the film thickness is reduced from 800 to 200 nm. The thermal response shows clear acoustic bumps due to strain. The value calculated for longitudinal sound velocity for Nb is 4247±72 ms^{-1}, which is within the range (3480–4900 ms^{-1}) previously reported [27].

REFERENCES

[1] P. Kneisel et al., "Review of ingot niobium as a material for superconducting radiofrequency accelerating cavities", Nucl. Instrum. Methods Phys. Res. A, vol. 774, p. 133, 2015. doi:10.1016/j.nima.2014.11.083

[2] R. L. Geng, H. Padamsee, A. Seaman, and V. D. Shemelin, "World record accelerating gradient achieved in a superconducting niobium rf cavity", in: Proc. 21st IEEE Particle Accelerator Conference, Tennessee, USA, May 2005, pp. 653-655. doi:10.1109/PAC.2005.1590516

[3] G. Myneni et al., "Medium grain niobium SRF cavity production technology for science frontiers and accelerator applications", JINST vol. 18, P. T04005, 2023. doi:10.1088/1748-0221/18/04/t04005

Content from this work may be used under the terms of the CC BY 4.0 licence (© 2024). Any distribution of this work must maintain attribution to the author(s), title of the work, publisher, and DOI.

ISBN: 978-3-95450-247-9 ISSN: 2673-5490 doi: 10.18429/JACoW-IPAC2024-THPR63

© Content from this work may be used under the terms of the CC BY 4.0 licence (© 2024). Any distribution of this work must maintain attribution to the author(s), title of the work, publisher, and DOI.

[4] H. Padamsee, "The science and technology of superconducting cavities for accelerators", Supercond. Sci. Technol, vol. 14, p. R28, 2001. doi:10.1088/0953-2048/14/4/202

[5] G. Rosaz, A. Bartkowska, C. P. A. Carlos, T. Richard, and M. Taborelli, "Niobium thin film thickness profile tailoring on complex shape substrates using unbalanced biased High Power Impulse Magnetron Sputtering", Surf. Coat. Technol., vol. 436, p. 128306, 2022. doi:10.1016/j.surfcoat.2022.128306

[6] M. Li et al., "The investigation of chemical vapor deposited copper-based niobium films", Mater. Res. Express, vol. 8, p. 046402, 2021. doi:10.1088/2053-1591/abefb1

[7] M. Arzeo et al., "Enhanced radio-frequency performance of niobium films on copper substrates deposited by high power impulse magnetron sputtering", Supercond. Sci. Technol., vol. 35, p. 054008, 2022. doi:10.1088/1361-6668/ac5646

[8] M. O. Islam, G. R. Myneni, and H. E. Elsayed-Ali, "Time-domain thermoreflectance measurement of the thermal diffusivity of Nb thin films", Thin Solid Films, vol. 790, p. 140213, 2024. doi:10.1016/j.tsf.2024.140213

[9] K. M. Yoo et al., "Femtosecond thermal modulation measurements of electron-phonon relaxation in niobium", Appl. Phys. Lett., vol. 56, p. 1908, 1990. doi:10.1063/1.103042

[10] R. Cheaito, C. S. Gorham, A. Misra, K. Hattar and P. E. Hopkins, "Thermal conductivity measurements via time-domain thermoreflectance for the characterization of radiation induced damage", J. Mater. Res., vol. 30, p. 1403, 2015. doi:10.1557/jmr.2015.11

[11] J. K. Chen and J. E. Beraun, "Numerical study of ultrashort laser pulse interactions with metal films", Numer. Heat Transfer A, vol. 40, p. 1, 2001. doi:10.1080/104077801300348842

[12] M. Mihailidi, Q. Xing, K. M. Yoo and T. R. Alfano, "Electron-phonon relaxation dynamics of niobium metal as a function of temperature", Phys. Rev. B, vol. 49, p. 3207, 1994. doi:10.1103/PhysRevB.49.3207

[13] G. Cannelli, and G. B. Cannelli, "Thermal properties of Nb from acoustic and electrical resistivity measurements in the temperature range 60-340 K", J. Appl. Phys., vol. 47, p. 17, 1976. doi:10.1063/1.322341

[14] A. V. Feshchenco, O. P. Saira, J. T. Peltonen, and J. P. Pekola, "Thermal conductivity of Nb thin films at sub-kelvin temperature", Sci. Rep., vol. 7, p. 41728, 2017. doi:10.1038/srep41728

[15] Y. Yang et al., "Study on laser annealing of niobium films deposited on copper for RF superconducting cavities", Nuclear Inst. and Methods in Phys. Res. A, vol. 964, p. 163803, 2020. doi:10.1016/j.nima.2020.163803

[16] M. M. Rahman, H. E. Elsayed-Ali, "On-line thin film thickness monitor by pulsed laser photoacoustics", Optics and Laser in Engineering", vol. 139, p. 106482, 2021. doi:10.1016/j.optlaseng.2020.106482

[17] O. B. Wright, "Thickness and sound velocity measurement in thin transparent films with laser picosecond acoustics", J. Appl. Phys., vol. 71, p. 1617, 1992. doi:10.1063/1.351218

[18] S. Sandell et al., "Thermoreflectance techniques and Raman thermometry for thermal property characterization of nanostructures", J. Appl. Phys., vol. 128, p. 131101, 2020. doi:10.1063/5.0020239

[19] T. Q. Qiu and C. L. Tien, "Femtosecond laser heating of multi-layer metals-I. Experiments", Int. J. Heat Mars Transf., vol. 37, p. 2789, 1994. doi:10.1016/0017-9310(94)90396-4

[20] T. Q. Qiu, and C. L. Tien, "Heat transfer mechanism during short-pulse laser heating on metals", J. Heat Transfer, vol. 115, p. 835, 1993. doi:10.1115/1.2911377

[21] J. Hohlfeld et al., "Electron and lattice dynamics following optical excitation of metals", Chemical Phys., vol. 251, p. 237, 2000. doi:10.1016/S0301-0104(99)00330-4

[22] A. P. Caffrey, P. E. Hopkins, J. M. Kloph and P. M. Norris, "Thin film non-noble transition metal thermophysical properties", MICROSC. THERM., vol. 9, p. 365, 2005. doi:10.1080/10893950500357970

[23] J. Jiang, K. Parto, W. Cao and K. Banerjee, "Ultimate monolithic-3D integration with 2D materials: rationale, prospects, and challenges", IEEE J. Electron Devices Soc., vol. 7, p. 878, 2019. doi:10.1109/JEDS.2019.2925150

[24] D. Hazra et al., "Thickness dependent lattice expansion in nanogranular Nb thin films", J. Appl. Phys., vol. 103, p. 103535, 2008. doi:10.1063/1.2924332

[25] D. A. Polonyankin et al., "Research of niobium thin films with a predetermined thickness produced by RF magnetron sputtering", IOP Conf. Ser.: Mater. Sci. Eng., vol. 168, p. 012069, 2017. doi:10.1088/1757-899X/168/1/012069

[26] C. Thomsen, H. T. Grahn, H. J. Maris, and J. Tauc, "Surface generation and detection of phonons by picosecond light pulses", Phys. Rev. B, vol. 34, pp. 4129-4138, 1986. doi:10.1103/physrevb.34.4129

[27] I. L. Shabalin, "Niobium", Ultra-High Temperature Materials I, Dordrecht, Netherlands, Springer, 2014, pp. 531-607. doi:10.1007/978-94-007-7587-9